Thermal Stress Emulation of Power Devices Subject to DFIG Wind Power Converter

# Thermal Stress Emulation of Power Devices Subject to DFIG Wind Power Converter

Yu, Xinming; Iannuzzo, Francesco; Zhou, Dao

*Published in:*
PEDG 2023 - 2023 IEEE 14th International Symposium on Power Electronics for Distributed Generation Systems

*DOI (link to publication from Publisher):*
10.1109/PEDG56097.2023.10215162

*Publication date:*
2023

*Document Version*
Accepted author manuscript, peer reviewed version

# Thermal Stress Emulation of Power Devices Subject to DFIG Wind Power Converter

Xinming Yu
Department of Energy
Aalborg University
Aalborg, Demark
xiyu@energy.aau.dk

Francesco Iannuzzo
Department of Energy
Aalborg University
Aalborg, Demark
fia@energy.aau.dk

Dao Zhou
Department of Energy
Aalborg University
Aalborg, Demark
zda@energy.aau.dk

***Abstract*—The turbine system equipped with doubly-fed induction generation (DFIG) is widely used in wind power generation. Due to the increasing focus on its prolonged lifespan, it is particularly important to ensure the accurate thermal stress estimation and system reliability in the industrial field. This paper mainly focuses on the thermal stress and lifetime of power semiconductor devices used in DFIG back-to-back converters and its mission profile emulator H-bridge converter. By setting different loading profiles, the power consumption, as well as the junction temperature of the devices in the DFIG power converter is compared with the H-bridge emulator. Through lifetime model of the power device, the lifespan can be calculated according to the annual wind profile. PLECS simulation is applied to verify the comparison between the DFIG power converter and H-bridge converter.**

***Keywords—Thermal stress emulation, DFIG, H-bridge, PLECS, lifetime***

## I. INTRODUCTION

Global Wind Energy Council (GWEC) expects that over 315 GW of new offshore wind capacity will be added over the next decade (2022-2031), bringing total global offshore wind capacity to 370 GW by the end of 2031 [1]. The doubly-fed induction generation (DFIG) is the mainstream model currently applied in wind farms, which has a wide range of speed operations with super-synchronous and sub-synchronous modes. The capacity of back-to-back converter is relatively small compared to the generator, leading to its cost-effective from the viewpoint of economic. The rotor of the DFIG is linked to the power grid by the rotor-side converter (RSC) and the grid-side converter (GSC) due to their positions, while the stator side is directly connected to the grid. The GSC keeps the DC bus voltage fixed and meets the reactive power demand according to the grid codes, while the RSC can produce active power to the power grid by following maximum power point tracking (MPPT), and provide the exciting current for the DFIG [2], [3].

The DFIG is typically controlled through the coordinate transformation, which gives the possibility to control its active and reactive power independently. The vector control is commonly used, including the stator voltage orientation and stator flux orientation [4]-[7]. If the stator voltage orientation is applied, the synchronous rotating frame is aligned with the stator voltage.

The key to investigate the reliability of DFIG power converter is to understand its failure mechanisms, where thermal-mechanical stress related degradation is dominant for module-based power semiconductors. Due to the different features and complex control strategies of the back-to-back power converter, a simplified emulator is needed to efficiently simulate the loading conditions and obtain the equivalent thermal stress of the wind power converter. Therefore, it is necessary to establish the theoretical models and compare the thermal stress of the emulator. At present, long-term thermal stress assessment from the field operation of renewable generation system is difficult and time consuming. Nevertheless, using H-bridge to simulate thermal stress of DFIG converters could be a promising approach.

The structure of the paper is as follows. Section II compares the topology structure and operating principle of the DFIG and H-bridge systems, where the equivalent circuits are introduced. Loss model and thermal model are described in Section III. Section IV presents thermal stress comparison between the DFIG and H-bridge systems, including theoretical calculations, the simulation verification. Section V estimates the lifespan of the power semiconductor based on the lifetime model. Finally, some conclusions are drawn in Section VI.

## II. CONTRAL AND PRINCIPLE OF DFIG AND EMULATOR

### A. DFIG topology and its control

As shown in Fig. 1, a typical DFIG topology consists of a generator, a partial-scale back-to-back power converter, a DC-link capacitor bank, and a filter inductor. The GSC and RSC can be controlled independently, and the grid voltage-oriented control (VOC) is adopted in this paper.

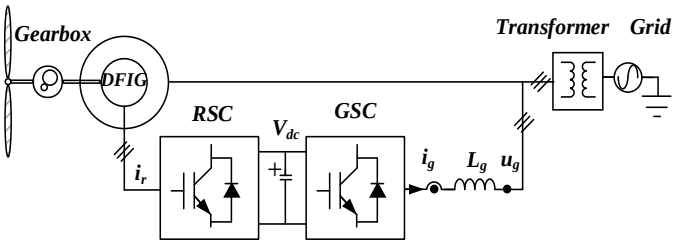


Fig. 1. DFIG topology with back-to-back converter.

To simplify the study, this paper takes GSC as an example for analysis and evaluation. As shown in Fig. 2, the GSC control strategy contains both grid current inner loop and power/voltage outer loop. Independent control of active and reactive power can be realized through d-axis and q-axis current decoupling. It is

Supported by the China Scholarship Council (No. 202207940010).

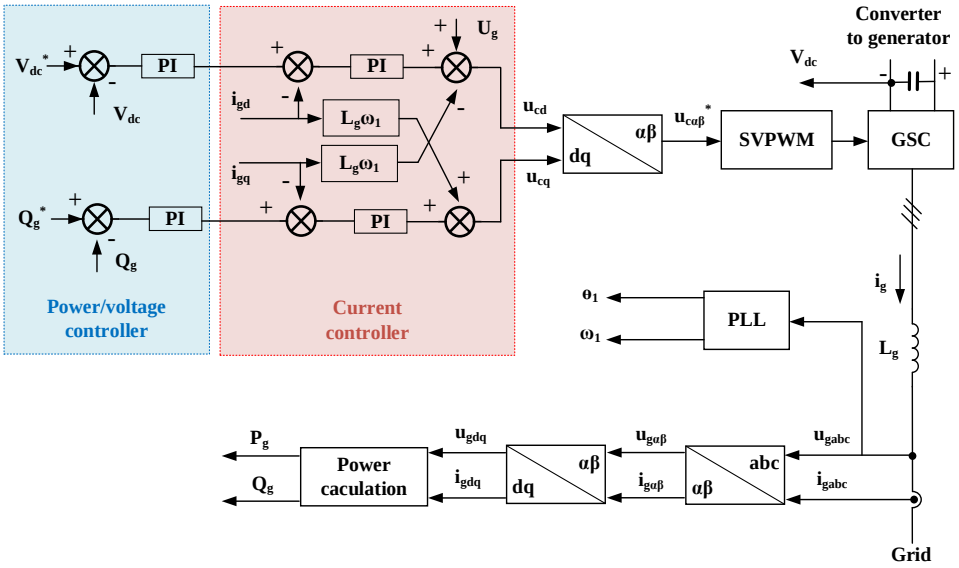


Fig. 2. Control scheme of the grid-side converter for the DFIG system.

noted that the GSC transfers the rotor power stored in the DC-link capacitors to the grid and maintains the DC-link voltage with a fixed value.

### B. DFIG GSC model

As shown in Fig. 3, the d-axis is aligned with the supply

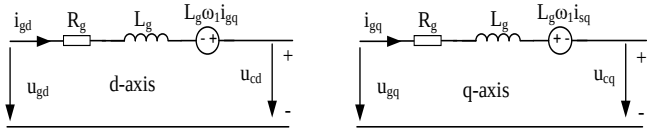


(a) (b)

Fig. 3. Equivalent circuit of GSC for DFIG system under synchronous reference frame. (a) d-axis circuit. (b) q-axis circuit.

voltage angle, the equivalent circuit of GSC under d-axis and q-axis can be deduced. Therefore, the relationship between the output voltage and current of the converter can be presented respectively as,

$$u_{cd} = u_{gd} - R_g i_{gd} - L_g \frac{di_{gd}}{dt} + \omega_1 L_g i_{gq} \quad (1)$$

$$u_{cq} = u_{gq} - R_g i_{gq} - L_g \frac{di_{gq}}{dt} - \omega_1 L_g i_{gd} \quad (2)$$

where $u_c$ and $u_g$ denote the converter and grid voltage, $R_g$ denotes the grid equivalent filter resistance. $L_g$ denotes the filter inductance. The subscripts $d$ and $q$ represent the d-axis and q-axis variables, respectively.

According to DFIG current decoupling control, the output active power and reactive power of the grid-side converter can be expressed by,

$$P_g = \frac{3}{2} U_g i_{gd} \quad (3)$$

$$Q_g = -\frac{3}{2} U_g i_{gq} \quad (4)$$

where $P_g$ and $Q_g$ denote the active and reactive power of GSC converter. Based on (3), the active power is only related to the d-axis grid current. Meanwhile, under the condition of unity power factor, the reactive power is zero, the q-axis reference current is set to zero.

### C. H-bridge system and its control

The single-phase H-bridge circuit is shown in Fig. 4, which consists of a test leg, a load leg, and an inductor. The driving signals of upper and lower switches are complimentary.

For the half-bridge configures, it is worthwhile to note that the loss dissipation of the power device is determined by the voltage and current profile of the converter output. In order to emulate the identical stress of the test leg from the DFIG power converter, the control objective of the test leg is to provide the same voltage stress or modulate index from the dc-link voltage, while the loading current of the test leg is regulated by close-loop current control, which provides the driving signals to the load leg.

As shown in Fig. 4 regarding the control circuit, in the test leg the IGBT $T_{1/2}$ is driven by $PWM_{1/2}$ generated by dq axis reference voltage, which emulates the identical modulation index of the GSC. The IGBT $T_{3/4}$ is controlled by the reference current dq axis, which comes from current reference of the GSC. Moreover, the load current $I_l$ needs to be delay for 1/4 period in order to achieve dq-axis control for a single-phase converter. Since the reference voltage, reference current and the displacement angle be flexibility configured, the H-bridge system is able to simulate the field operating environment of power devices that used in the GSC. As the running state of the test leg can be emulated under different working conditions, the power dissipation, and junction temperature swing can be estimated.

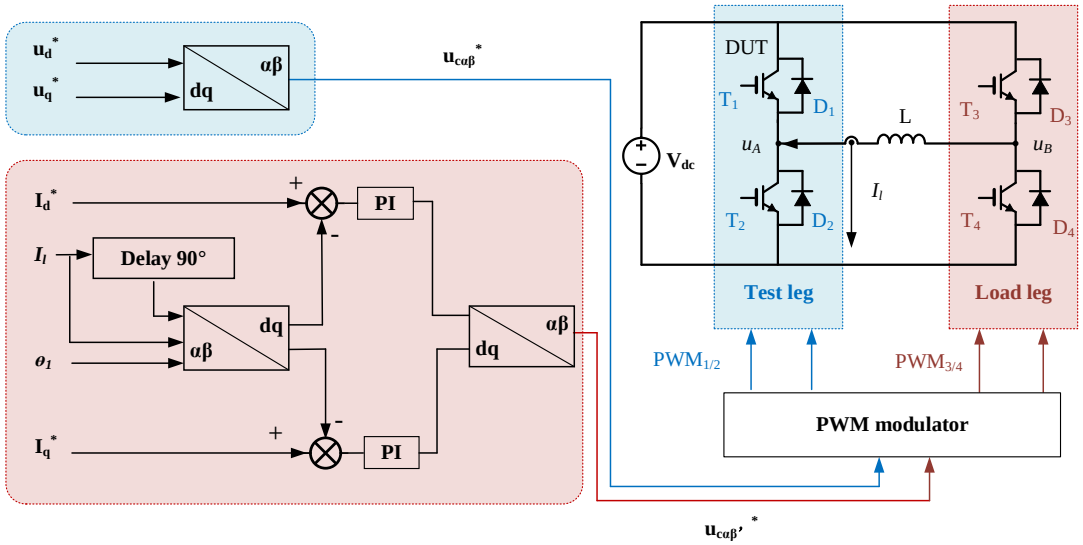


Fig. 4. Control scheme of the H-bridge converter system.

### D. H-bridge model

For the convenience of calculation, the simplified H-bridge circuit is shown in the Fig. 5, where the current inflow is

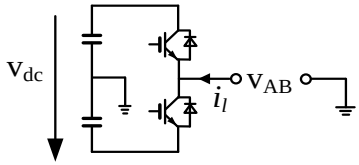


Fig. 5. Output voltage at bridge arm.

positive. As current needs to be the same direction during a half period, assuming converter output current $i_L(t)$ and voltage $u_{AB}(t)$:

$$i_L(t) = I_l \sin(\omega t) \tag{5}$$

$$u_{AB}(t) = U_{AB} \sin(\omega t - \varphi) \tag{6}$$

$$M = \frac{U_{AB}}{V_{dc}/2} \tag{7}$$

By using SPWM, the duty cycle is:

$$d(t) = \frac{1}{2}(1 + M\, sin(\omega t - \varphi)) \tag{8}$$

where $i_l$ and $u_{AB}$ denote the converter inductor current and output voltage, $I_l$ and $U_{AB}$ denote peak value (the current and voltage correspond to the output phase current and voltage by the GSC converter). $\varphi$ is displacement angle of the $i_l$ and $u_{AB}$. $M$ denotes the voltage modulation index.

## III. Loss Model and Thermal Model

The power dissipation of GSC converter and H-bridge power device mainly includes conduction loss and switching loss. Under specific wind speed conditions, the turbine will generate specific frequency, voltage, current and displace angle in order to maintain maximum power point tracking. linear approximation of the IGBT forward characteristics is assumed, the conduction loss $P_T$ can be further simplified as:

$$P_T = \frac{1}{2}\left(\frac{1}{\pi} V_{CE0} I_l + \frac{1}{\pi} V_{CE0} I_l^2\right) + M\cos\varphi\left(\frac{1}{8} V_{CE0} I_l + \frac{1}{3\pi} V_{CE0} I_l^2\right) \tag{9}$$

where $V_{CE0}$ means the collector-emitter initial voltage drop, $M$ is the modulation index, $I_l$ denotes the peak value of output current.

To facilitate calculation of switching loss, the polynomial fitting method is used to represent the switching loss the IGBT. According to the relationship between energy and power dissipation, the sum of turn-on loss and turn-off loss is the switching loss. The switching loss $P_{swT}$ in a fundamental period can be calculated as following:

$$P_{swT} = f_{\_sw} \frac{V_{dc}}{V_{dc}^*}\left(\frac{a_T}{2} + \frac{b_T}{\pi} I_l + \frac{c_T}{4} I_l^2\right) \tag{10}$$

where $f_{\_sw}$ is switching frequency. $V_{dc*}$ denotes reference voltage. $a_T$, $b_T$, $c_T$ denote the corresponding coefficient of the fitting function respectively. The above three parameters are obtained by MATLAB fitting according to the worst junction temperature (150°C) in the datasheet. The diode switching loss model is the same as that of the IGBT, but the switching loss only includes the turn-off loss.

The thermal impedance of power module is shown in Fig. 6. The relationship between mean junction temperature $T_{j\_T}$ and junction temperature swing $\Delta_{Tj\_T}$ can be obtained as follows:

$$T_{j\_T} = P_T\left(\sum_{i=1}^{4} R_{thJC\_T}(i) + R_{thCH\_T}\right) + (P_T + P_D) * R_{thHA} + T_a \tag{11}$$

where $T_{j\_T}$ stands for chip surface temperature, $T_{c\_T}$ indicates the case temperature, $T_h$ denotes heatsink temperature, and $T_a$ means ambient temperature. Moreover, $t_{on}$ denotes a half of

fundamental period and $T$ is the fundamental period of the load current. $\tau$ denotes the thermal time constant of each Foster network.

$$\Delta T_{j\_T}=2P_T*\sum_{i=1}^{4}R_{thJC\_T}(i)*\frac{\left(1-e^{\frac{-t_{on}}{\tau_{thJC\_T}i}}\right)^2}{1-e^{\frac{-T}{\tau_{thJC\_T}i}}}t \qquad (12)$$

In general, in order to facilitate calculation, the junction-to-case RC network will be converted into fourth-order Foster

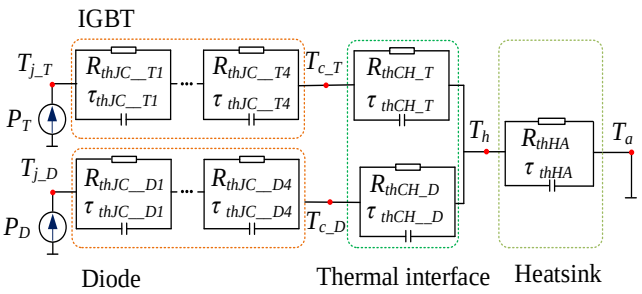


Fig. 6. Thermal impedance model of power module.

model under the same thermal effect conditions.

## IV. Thermal Stress Comparison between DFIG and H-bridge Systems

In this section, the simulated loss dissipation and thermal cycling of the power device will be presented and compared with mathematical calculations from the loss and thermal models. A case study of 2 MW DFIG system is carried out. Some important parameters of the wind turbine are used in Table I, with dc-link voltage of 1200 V, and switching frequency of 2 kHz. Moreover, Danfoss P3 power module is selected [8]. The parameters of H-bridge and DFIG are summarized in Table II and Table III, respectively.

TABLE I. PARAMETERS FOR WIND TURBINE

| Specification | Value | Specification | Value |
|---|---|---|---|
| Rated power | 2 MW | Blade radius | 41.3 m |
| Cut-in wind speed | 4 m/s | Cut-off wind speed | 25 m/s |
| Rated wind speed | 12 m/s | Optimal tip speed ratio | 8.1 |
| Maximun power coefficient | 0.41 | Gearbox speed ratio | 26 |

TABLE II. PARAMETERS AND CONDITIONS OF H-BRIDGE SYSTEM

| Specification | Value | Specification | Value |
|---|---|---|---|
| Power module | P3 | Power factor | -1 |
| DC voltage | 1200 V | Voltage modulation ratio | 0.94 |
| Filter inductor | 0.3 mH | Fundamental frequency | 50 Hz |
| Reference voltage $U_d$ | 562.3 V | Switching frequency | 2 kHz |
| Rreference voltage $U_q$ | 61.9 V | Proportional coefficient $K_p$ | 0.1 |
| Reference current $I_d$ | 394 A | Integral coefficient $K_i$ | 10 |
| Reference current $I_q$ | 0 A | | |

TABLE III. PARAMETERS AND CONDITIONS OF DFIG AND POWER CONVERTER

| Specification | Value | Specification | Value |
|---|---|---|---|
| Power module | P3 | Voltage modulation ratio | 0.94 |
| DC-link voltage $U_{dc}$ | 1200 V | Fundamental frequency | 50 Hz |
| Grid voltage $U_g$ | 563 V | Switching frequency | 2 kHz |
| Filter inductance $L_g$ | 0.5 mH | Current proportional coefficient $K_{ip}$ | 0.45 |
| Stator resistance $R_s$ | 1.688 mΩ | Current integral coefficient $K_{ii}$ | 4.5 |
| Stator leakage inductance $L_s$ | 0.038 mH | Voltage proportional coefficient $K_{up}$ | 50 |
| Rotor leakage inductance $L_r$ | 0.064 mH | Voltage integral coefficient $K_{ui}$ | 180 |
| Magnetizing inductance $L_m$ | 2.91 mH | | |

Fig. 7(a) shows the filtered output voltage and current of the DFIG GSC from the PLECS simulation. Voltage and current displacement angle can be obtained by time difference at the zero-crossing. According to amplitude of voltage, current and its displacement angle, the power consumption of corresponding device can be obtained. he simulation results of the H-bridge system can be obtained by knowing the operation conditions from the GSC, which is shown in Fig. 7(b).

Fig. 8(a) presents the power loss of power device in the GSC. Meanwhile, the junction temperature can be obtained by knowing the thermal resistance of the power device. Under the same condition (wind speed 12 m/s), $U_d$ and $U_q$ are 562.3 V, 61.9 V respectively. $I_d$ and $I_q$ are -394 A, 0 A respectively. The slip frequency is 10 Hz, and the fundamental frequency is 50 Hz.

Fig. 8(a) and Fig. 8(b) show the DFIG IGBT total loss and diode total loss are 398 W and 193 W, respectively. The DFIG average junction temperature of IGBT and diode is 61.1 °C and 60.8 °C, respectively. IGBT and diode junction temperature fluctuations are 11.2 °C and 11.5 °C, respectively.

Comparing Fig. 7 and Fig. 8, under the same reference voltage, current and displace angle conditions, the DFIG and H-bridge systems can produce the same power dissipation, junction temperature, and junction temperature fluctuation. Therefore, H-bridge system can be used to simulate the thermal stress of power devices of DFIG.

To evaluate all the loading conditions of the DFIG power converter, the wind speed from the cut-in value (4 m/s) to the rated value (12 m/s) are taken into account. Fig. 9(a) is the output voltage and current of the two systems, respectively. It can be clearly seen that the trend of two systems regarding the voltage and current changing with wind speed is the same. The output voltage remains constant, while the current increases and then decreases before the sub-synchronous speed, and the current increases and remains constant in the super-synchronous state. Fig. 9(b) shows the power loss of the two systems. For the two systems, the power loss trend of the IGBT and diode power devices is consistent with the change trend of the loading current. Fig. 9(c) presents a comparison of the average junction temperature. In sub-synchronous state the diode junction temperature is higher, as the power converter is in the

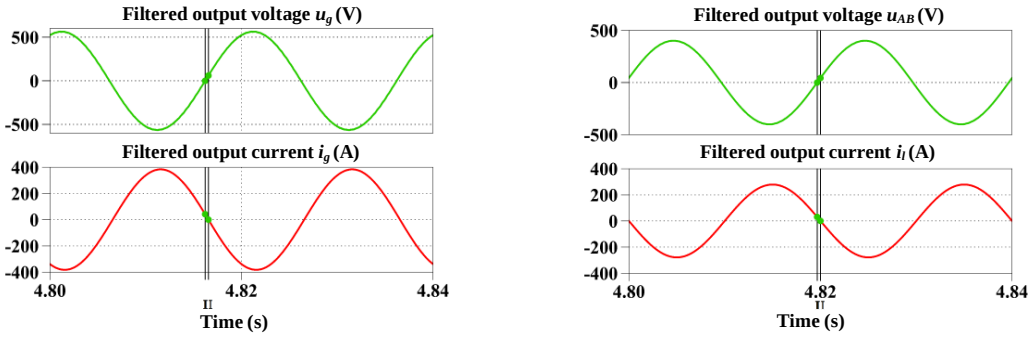


(a) (b)

Fig. 7. PLECS simulation output voltage and current of IGBT and diode with 12 m/s wind speed. (a) DFIG GSC system. (b) H-bridge system.

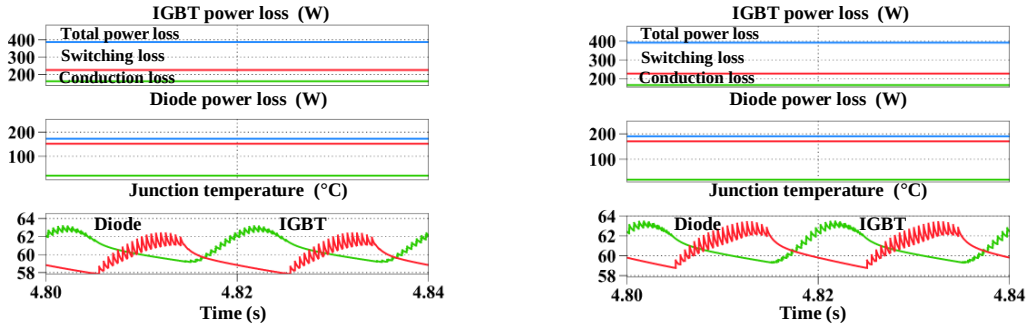


(a) (b)

Fig. 8. PLECS simulation power loss and junction temperature of IGBT and diode with 12 m/s wind speed. (a) DFIG GSC system. (b) H-bridge system.

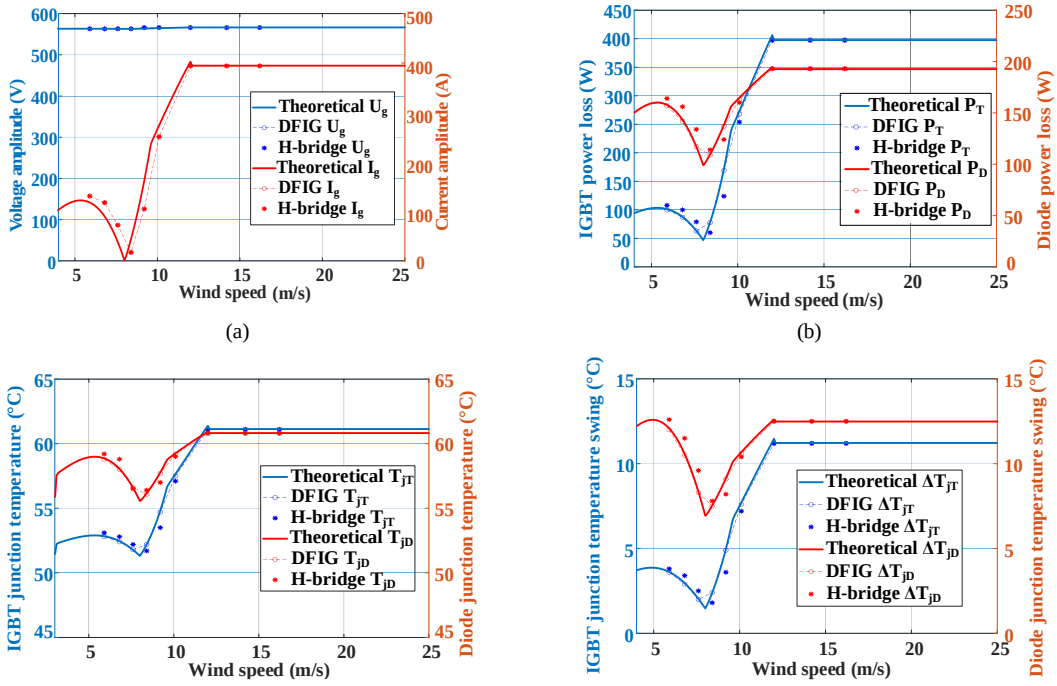


(a) (b)

(c) (d)

Fig. 9. Theoretical result and PLECS simulation comparison between DFIG GSC and H-bridge system of IGBT and diode power device under different wind speed. (a) Output voltage and current. (b) Power loss. (c) Mean junction temperature. (d) Junction temperature swing.

rectification state. In the super-synchronous state, the IGBT has a higher power loss. Fig. 9(d) compares the junction temperature fluctuation between IGBT and diode. The diode junction temperature fluctuates greatly under the same wind speed conditions, because the junction temperature fluctuation is not only affected by the power consumption of the power device, but also affected by the thermal resistance.

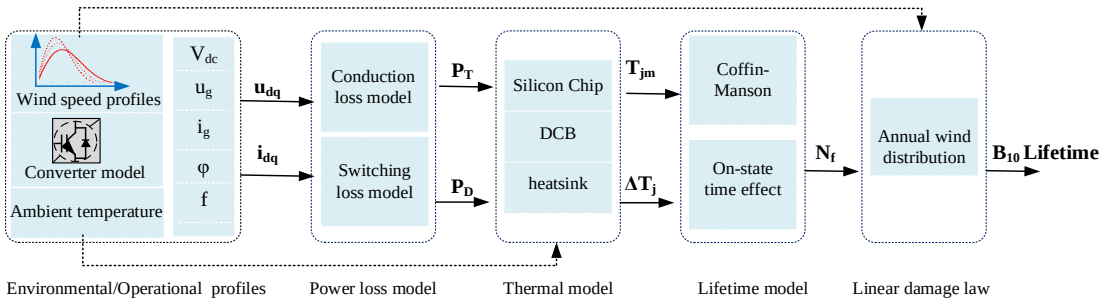


Fig. 10. Mission profile-based assessment procedure for wind power converter reliability.

## V. Lifetime Estimation of Power Devices

Fig. 10 shows the procedure to assess wind power converter reliability based on the mission profile. With the different wind speeds, the DFIG rotor speed and power also change (this paper mainly focuses on the change of the DFIG from sub-synchronous state to super-synchronous state during the change of wind speed from 4 m/s to 12 m/s). In this process, the output voltage, current and corresponding displacement angle of the GSC converter change with the wind speed, and the power consumption and thermal stress of the power device in different states are calculated. Afterwards, the power cycle to failure $N_f$ can be obtained according to the Coffin-Manson lifetime model. Finally, with the annual wind speed distribution, the $B_{10}$ lifetime of the converter can be obtained. In this process, a linear damage accumulation in the fatigue is assumed. Moreover, this paper assumes a unified failure mechanism.

According to the Coffin-Manson model, the $B_{10}$ lifetime formula of the IGBT is as following:

$$N_{f\_T} = 1.27 * 10^6 * \Delta T_{j\_T}{}^{-5.039} * e^{\frac{7166.7}{273+T_{j\_T}}} * \left(\frac{t_{on}}{0.7}\right)^{-0.463} \quad (13)$$

where $t_{on}$ denotes half of the loading current period.

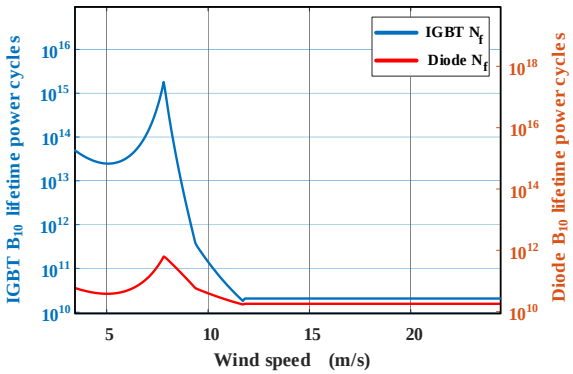


Fig. 11. $B_{10}$ lifetime power cycles comparison of power semiconductors.

According to the parameters given by the manufacturer, the Coffin-Manson lifetime model of the power device can roughly be established [9], the relationship between the number of $B_{10}$ power cycles and the corresponding wind speed can be calculated, as shown in Fig. 11. The power cycle to failure of the diode in the sub-synchronous period is much lower than that of the IGBT, while the power cycles to failure of the two power devices in the super-synchronous period is close. Under the same wind speed condition, it can be expected that the lifetime of IGBT is longer.

For a wind energy conversion system, it can almost be regarded that the wind profile appears periodically every year , the annual $CL_T$ can be calculated by dividing the total number of cycles per year by the $B_{10}$ lifetime estimated.

$$CL_T = \frac{f\_v*365*24*3600*f}{N_{f\_T}} \quad (14)$$

where $f_{\_v}$ denotes the annual percentage of every wind speed, here the value is 0.95. $f$ denotes the fundamental frequency.

It is obvious that the total annual lifetime consumption of the two power devices under all wind speed conditions can be calculated according to the $CL_T$, as shown in Fig. 12.

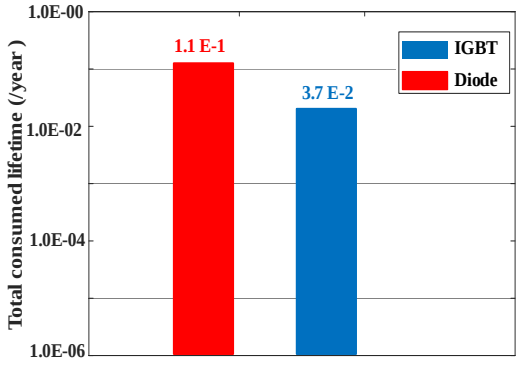


Fig. 12. Total consumed lifetime comparison of power semiconductors.

$$TCL_T = \sum_{n=4}^{25} CL_T \quad (15)$$

If the Class-I wind profile is selected [3], the total consumed lifetime (TCL) can be estimated. To compare the annual IGBT and diode consumed lifetime, the diode annual consumed lifetime is 2.7 times that of the IGBT. It can be seen that the annual lifetime consumption of the IGBT is 3.7E-2, which indicates the IGBT lifetime of 27 years.

## VI. CONCLUSION

This paper demonstrates that the H-bridge system is able to emulate thermal stress of DFIG power converter identically under various loading conditions. Comparative analysis of theoretical calculation and simulation of the two systems, DFIG and H-bridge power converters with the same voltage, current, power factor, DC-link voltage, modulation index will have the same power consumption and thermal stress. Comparing the sub-synchronous and super-synchronous operating states, under sub-synchronous conditions, the IGBT suffers less thermal stress than the diodes, and its power cycle to failure is longer. In the super-synchronous state, the thermal stress of the two power devices is close, so the $B_{10}$ power cycle to failure is also similar. Compared with two power devices, the annual lifetime consumption of the diode is higher.

## REFERENCES


[1] R. Williams, F. Zhao, and J. Lee. Global Wind Energy Council. Web. 29 June 2022. https://gwec.net/wp-content/uploads/2022/06/GWEC-Offshore-2022_update.pdf.

[2] F. Blaabjerg. *Control of Power Electronic Converters and Systems*, Volume 2. Vol. 2. Academic Press, 2018.

[3] D. Zhou, F. Blaabjerg, T. Franke, M. Toennes, and M. Lau "Comparison of Wind Power Converter Reliability with Low-Speed and Medium-Speed Permanent-Magnet Synchronous Generators," *IEEE Trans. Ind Electron.*, vol. 62, no. 10, pp. 6575-6584, Oct. 2015.

[4] F. Blaabjerg, and K. Ma, "Future on power electronics for wind turbine systems," *IEEE Trans. Emerging Sel. Topics Power Electron.*, vol. 1, no. 3, pp. 139–152, Sep. 2013.

[5] Z. Chen, J. M. Guerrero, and F. Blaabjerg, "A review of the state of the art of power electronics for wind turbines," *IEEE Trans. Power Electron.*, vol. 24, no. 8, pp. 1859–1875, Aug. 2009.

[6] K. Ma, M. Liserre, F. Blaabjerg, and T. Kerekes, "Thermal Loading and Lifetime Estimation for Power Device Considering Mission Profiles in Wind Power Converter," *IEEE Trans. on Power Electron*., vol. 30, no. 2, pp. 590-602, Feb. 2015.

[7] K. Ma, S. Jiang, E. Li and X. Cai, "Three-Phase Mission Profile Emulator for Multiple Submodules in Modular Multilevel Converter," *IEEE Trans. on Power Electron*, vol. 36, no. 5, pp. 5213-5222, May 2021.

[8] Danfoss "Technical information for IGBT module DP 1000B1700T 103717Datasheet" https://acrobat.adobe.com/link/review?uri=urn:aaid:scds:US:d7645a3e-1f55-3281-94cb-0965865eb10d.

[9] Wintrich, U. Nicolai, and T, Reimann, *Application Manual*, Semikron, Nuremberg, Germany, 2011.